

Jet properties from $\pi^\pm - h^\pm$ correlation in $p + p$ and $d + \text{Au}$ collisions at $\sqrt{s_{NN}} = 200 \text{ GeV}$

Jiangyong Jia[†] for the PHENIX Collaboration

[†] Columbia University, New York, NY 10027 and Nevis Laboratories, Irvington, NY 10533, USA

E-mail: jjia@nevis.columbia.edu

Abstract. We review recent results on the charged pion - charged hadron correlation in $p + p$ and $d + \text{Au}$ collisions as measured by the PHENIX Collaboration. Properties of di-jet system, such as the jet shape, associated hadron yield per trigger pion, and the underlying event are extracted statistically from the $\pi^\pm - h^\pm$ correlation function in $\Delta\phi$ and $\Delta\eta$. For jet triggered with high p_T pions ($p_T > 5 \text{ GeV}/c$), no apparent differences in the jet properties are seen between $p + p$ and $d + \text{Au}$.

1. Introduction

The technique of two particle correlation in relative azimuth ($\Delta\phi$) and pseudorapidity ($\Delta\eta$) is an useful tool to access the (di-)jet properties in heavy-ion collisions. Comparing with the traditional full jet reconstruction method, the two particle correlation method is relatively insensitive to the level of the underlying event, thus can probe soft jets ($\lesssim 5 \text{ GeV}/c$); combining with event mixing technique, it can also be used for detectors with limited acceptance.

To leading order in QCD, high p_T jets are produced back-to-back in azimuth. This back-to-back correlation, however, is smeared by the fragmentation process and the initial and final state radiation, which lead to a typical di-hadron correlation function in $\Delta\phi$ as shown schematically in Figure.1. The associated hadron yield per trigger π^\pm (conditional yield or CY) can be parameterized by a constant plus a double gauss function,

$$\frac{1}{N_{\text{trig}}^0} \frac{dN_0}{d\Delta\phi} = B + \frac{N_S}{\sqrt{2\pi}\sigma_N} e^{-\frac{\Delta\phi^2}{2\sigma_N^2}} + \frac{N_A}{\sqrt{2\pi}\sigma_F} e^{-\frac{(\Delta\phi-\pi)^2}{2\sigma_F^2}}, \quad (1)$$

In this analysis, everything about the (di-)jet is extracted from this parameterization. The peaks in the same side ($\Delta\phi = 0$) and the away side ($\Delta\phi = \pi$) represent the intra-jet and di-jet correlation, respectively. The widths of the peaks are controlled by the jet fragmentation momentum j_T and the parton transverse momentum k_T [1, 2]: $\sigma_{\text{same}} \propto j_{Ty}$, $\sqrt{\sigma_{\text{away}}^2 - \sigma_{\text{same}}^2} \propto k_{Ty}$, where the subscript “y” represent the 1D projection in transverse plane; The integrals of the peaks, N_S and N_A give the total number of hadrons associated with the trigger hadrons in the same side and the away side; The pedestal level beneath the jet structure, B , represents contributions from the underlying event.

The presence of the medium can modify the di-hadron correlation. Recent results from RHIC [3, 4, 5] and SPS [6] indicate a complicated modification of the jet structure in both

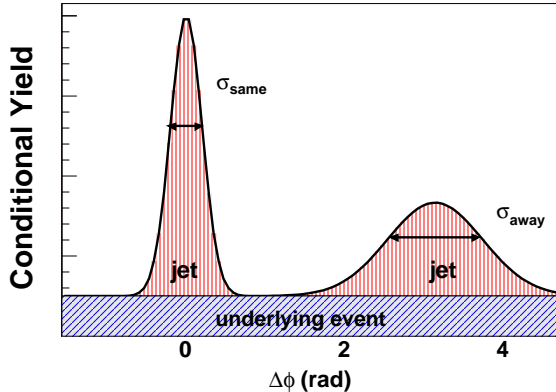


Figure 1. Cartoon of the two particle $\Delta\phi$ correlation. The yield of hadron per trigger (Conditional Yield) has a di-jet part and a part corresponding to the underlying event.

the same side and the away side. The same side jet become elongated in $\Delta\eta$ but is relatively unmodified in $\Delta\phi$ direction. Meanwhile, the away side correlation become much broader and suppressed, which indicates strong interaction of the jets with the dense medium. In order to achieve quantitative understandings of the modifications of jets in the medium, one has to obtain an accurate baseline measurements of jet correlation in $p + p$ and $p + A$ collisions. Di-hadron correlation in $p + p$ collisions probes basic QCD effects such as jet fragmentation, initial and final state radiations; while correlation in $p + A$ collisions gives handle on the various initial state effects such as shadowing and jet broadening in cold nuclear medium.

We focus the physics discussions on three aspects of the $\pi^\pm - h^\pm$ correlations in Figure.1: jet shape, jet yield and the underlying event. But before doing that, we briefly discuss the identification of high p_T charged pion and the techniques used to extract the jet properties.

2. Analysis

2.1. π^\pm identification

PHENIX identifies high momentum charged pions with the RICH and EMCal detectors. Charged particles with velocities above the Cherenkov threshold of $\gamma_{\text{th}} = 35$ (CO_2 radiator) emit Cherenkov photons, which are detected by photo-multiplier tubes (PMTs) in the RICH [7]. This threshold corresponds to 18 MeV/ c for electrons, 3.5 GeV/ c for muons and 4.9 GeV/ c for charged pions. In a previous PHENIX publication [8], we have shown that charged particles with reconstructed p_T above 4.9 GeV/ c , which have an associated hit in the RICH, are dominantly charged pions and background electrons from photon conversions. The efficiency for detecting charged pions rises quickly past 4.9 GeV/ c , reaching an efficiency of $> 90\%$ at $p_T > 6$ GeV/ c .

To reject the conversion backgrounds in the pion candidates, the shower information at the EMC is used. Since most of the background electrons are genuine low p_T , they can be rejected by requiring a large shower energy in the EMC. In this analysis, a momentum dependent energy cut at EMC is applied: $E > 0.3 + 0.15p_T$. Additional electron rejection comes from the χ^2 variable,

$$\chi^2 = \sum_i \frac{(E_i^{\text{meas}} - E_i^{\text{pred}})^2}{\sigma_i^2} \quad (2)$$

where E_i^{meas} is the energy measured at tower i , E_i^{pred} is the predicted energy for an electromagnetic particle of total energy $\sum_i E_i^{\text{meas}}$ and σ_i is the standard deviation for E_i^{pred} .

Both E_i^{pred} and σ_i are obtained from the electron test beam data. EM shower is more compact than hadronic shower, thus has a smaller χ^2 value. The χ^2 value is then mapped to the probability ($prob$) for a shower being an EM shower. $prob$ ranges from 0 to 1, with a flat distribution expected for EM showers and a distribution peaked around 0 for hadronic showers. Figure. 2a shows the normalized $prob$ distribution for the pion candidates and electrons. A cut of $prob < 0.2$ selects pions with an efficiency of $\gtrsim 80\%$. Since we are interested in per-triggered yield, the detailed knowledge of the pion efficiency is not necessary. The raw pion spectra for requiring only RICH cut and both RICH and EMCal cuts are shown in Figure. 2b, the difference between the two is mostly due to electron background. The sample of charged pion used in the correlation analysis is from 5 to 16 GeV/c, with a purity better than 95%.

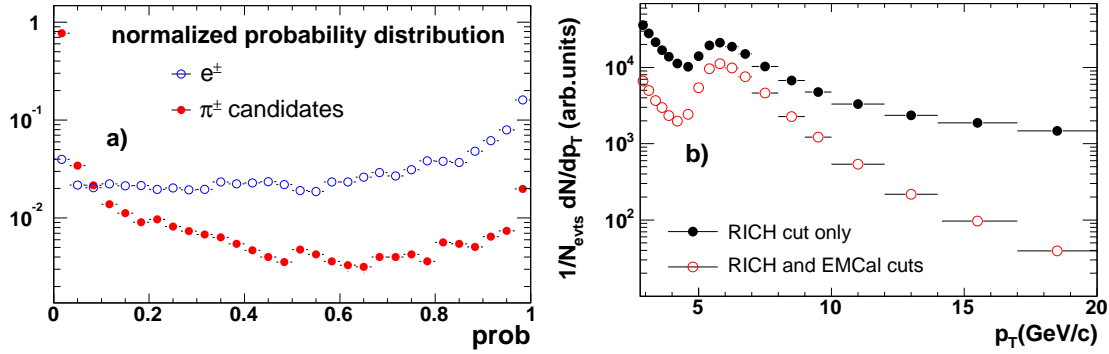


Figure 2. a) The probability distribution for charged pion candidates (solid circles) and electrons (open circles), where the integrals of the histograms have been normalized to one. b) Raw pion spectra with matching hit at RICH only (solid circles) and with both RICH and EMCal cuts (open circles).

2.2. Extracting jet properties

The correlation functions are generally defined as

$$C(\Delta\phi) = \frac{N_{\text{cor}}(\Delta\phi)}{N_{\text{mix}}(\Delta\phi)} \text{ in azimuth and } C(\Delta\eta) = \frac{N_{\text{cor}}(\Delta\eta)}{N_{\text{mix}}(\Delta\eta)} \quad (3)$$

in pseudorapidity. N_{cor} and N_{mix} represent the same-event pair distribution and mixed-event pair distributions, respectively. The mixing is done by pairing trigger π^\pm with charged hadrons from events having similar collision vertex and centrality as the π^\pm . Ref.[2] has shown that the correlation function and the conditional yield are related to each other by just a constant,

$$\frac{1}{N_{\text{trig}}^0} \frac{dN_0}{d\Delta\phi} = \frac{R_{\Delta\eta}}{N_{\text{trig}}\epsilon} \frac{N_{\text{cor}}(\Delta\phi)}{\int d\Delta\phi N_{\text{mix}}(\Delta\phi)} \quad (4)$$

where N_{trig}^0 and N_{trig} are the true and detected number of triggers respectively, and ϵ is the average single particle efficiency for the associated particles in 2π in azimuth and ± 0.35 in pseudo-rapidity. $R_{\Delta\eta}$ accounts for the loss of jet pairs outside PHENIX pair acceptance of $|\Delta\eta| < 0.7$.

The two gauss functions in Eq.1 describe the $\Delta\phi$ distribution of the jet signal. The jet signal can also be presented in any other pair variables, such as $\Delta\eta$, trigger p_T ($p_{T,\text{trig}}$), associated hadron p_T ($p_{T,\text{assoc}}$), $p_{\text{out}} = p_{T,\text{assoc}} \sin \Delta\phi$, $x_E = \frac{p_{T,\text{assoc}} \cos \Delta\phi}{p_{T,\text{trig}}}$, di-hadron mass and di-hadron

p_T . For every pair variable, we use a statistical weighting method to account for the acceptance correction. According to Eq.4, each pair on average needs a $\Delta\phi$ dependent correction factor, $w(\Delta\phi)$,

$$w(\Delta\phi) = \frac{BR_{\Delta\eta}}{N_{\text{trig}}\epsilon} \frac{1}{\int d\Delta\phi N_{\text{mix}}(\Delta\phi)} \quad (5)$$

When this factor is used as the weight in filling the x_E histograms for both real and mixed pairs, we obtain

$$\frac{1}{N_{\text{trig}}^0} \frac{dN_0}{dx_E} = \sum_{\text{real}} \delta(x_E) w(\Delta\phi) \quad (6)$$

for the same-event pair distribution. Thus according to Eq.1, x_E distribution for jet pairs equals to

$$\frac{1}{N_{\text{trig}}^0} \frac{dN_0^{\text{jet}}}{dx_E} = \sum_{\text{real}} \delta(x_E) w(\Delta\phi) - C \sum_{\text{mix}} \delta(x_E) w(\Delta\phi) \quad (7)$$

where

$$C = \frac{BR_{\Delta\eta}}{N_{\text{trig}}\epsilon} \frac{2\pi}{\int d\Delta\phi N_{\text{mix}}(\Delta\phi)} \quad (8)$$

Replacing x_E with any pair variables, we obtain other jet pair distributions. However, the integral of the jet yield should be conserved independent of the pair variable used, *i.e.*:

$$\int d\Delta\phi \frac{dN_0^{\text{jet}}}{d\Delta\phi} = \int dx_E \frac{dN_0^{\text{jet}}}{dx_E} = \int dp_{T,\text{assoc}} \frac{dN_0^{\text{jet}}}{dp_{T,\text{assoc}}} = \int dp_{\text{out}} \frac{dN_0^{\text{jet}}}{dp_{\text{out}}} \quad (9)$$

3. Results

3.1. Jet shape

In the following discussion, the trigger π^\pm p_T is always from 5 to 10 GeV/c, unless specified otherwise. Figure.3 shows the $\pi^\pm - h^\pm$ $\Delta\phi$ distribution from $p + p$ and $d + \text{Au}$ collisions for several range of $p_{T,\text{assoc}}$. The widths decrease with increasing $p_{T,\text{assoc}}$, which is consistent with narrowing of the jet cone for larger $p_{T,\text{assoc}}$. It is interesting to notice that a large fraction of all hadrons in the event are associated with the trigger, thus are originated from the hard-scattered partons. Even for $p_{T,\text{assoc}}$ as low as 0.4 – 1 GeV/c, about 51% hadron yield in $p + p$ (27% in $d + \text{Au}$) comes from the jet fragmentation.

Using the event mixing technique, we also measure the jet shape in η . For the single acceptance of $|\eta| < 0.35$, the pair acceptance in pseudorapidity is limited to be $|\Delta\eta| < 0.7$. Figure.4a shows the same event and mixed event $\Delta\eta$ distribution for $1 < p_{T,\text{assoc}} < 2$ GeV/c, where a cut of $|\Delta\phi| < 1$ is used to select only same side jet pairs. The mixed-event pair distribution is not a perfect triangle due to a gap around $\eta = 0$ in PHENIX central arm detectors. The ratio of the two distributions gives the jet shape in $\Delta\eta$. It is shown in Figure.4b and compared with the jet shape in $\Delta\phi$. There is no significant difference between the two and the extracted widths are consistent in both directions. We extend this comparison to other associated hadron p_T ranges and summarize the results in Figure.5. The overall agreement between the jet widths in $\Delta\eta$ and $\Delta\phi$ is pretty good, except at small $p_{T,\text{assoc}}$, where the width in $\Delta\eta$ is systematically lower than that in $\Delta\phi$. The fact that this discrepancy exist in both $p + p$

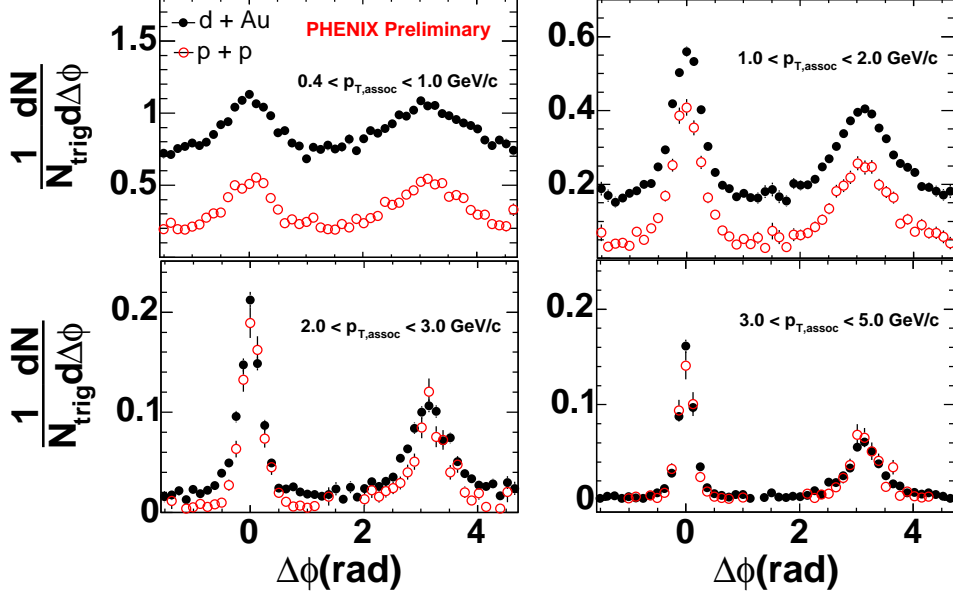


Figure 3. Corrected conditional pair distributions for $p+p$ and minimum bias $d+Au$ collisions. The trigger π^\pm are correlated with hadrons with $p_{T,assoc}$ 0.4–1.0 GeV/ c , 1.0–2.0 GeV/ c , 2.0–3.0 GeV/ c and 3.0 – 5.0 GeV/ c (from top to bottom and left to right).

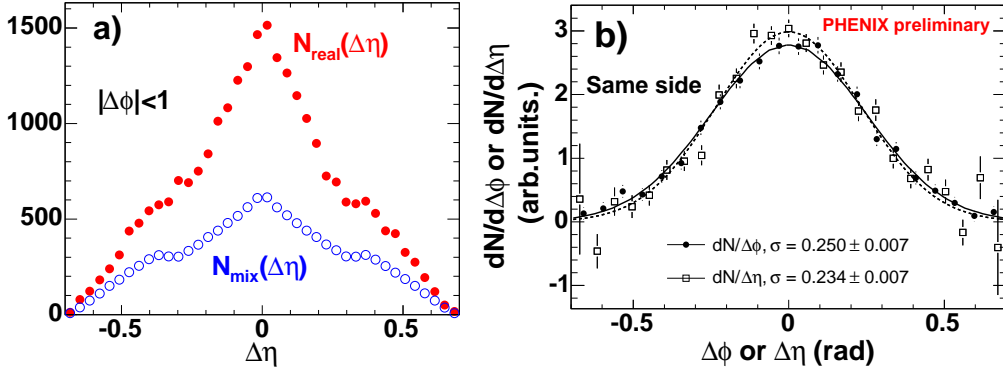


Figure 4. a) The same-event and mixed-event pair distribution in $\Delta\eta$, b) the correlation function in $\Delta\eta$ (open boxes) and $\Delta\phi$ (filled circles).

and $d + Au$ collisions indicates that this deviation is likely due to the systematics of the fitting in a limited $\Delta\eta$ range rather than any real physics effect in $d + Au$.

From the measured jet width, one can calculate the rms value of zk_{Ty} [2], $(zk_{Ty})_{RMS} = \sqrt{\langle z^2 k_{Ty}^2 \rangle}$, for both $p+p$ and $d + Au$. The resulting $(zk_{Ty})_{RMS}$ is plotted as function of trigger p_T in Figure.6. It looks quite similar between $p+p$ and $d + Au$. The difference of $(zk_{Ty})_{RMS}$, averaged over p_T , is $\langle z^2 k_{Ty}^2 \rangle_{dAu} - \langle z^2 k_{Ty}^2 \rangle_{pp} = 0.64 \pm 0.78 \pm 0.42$ (GeV/ c) 2 , which is consistent with 0. According to various theoretical estimations [9], the typical contribution to $\langle k_{Ty}^2 \rangle$ from multiple scattering is 1 (GeV/ c) 2 in central $d + Au$ collisions, while the contribution from initial and final radiation is much larger (around 8 (GeV/ c) 2) [10]. The small multiple scattering

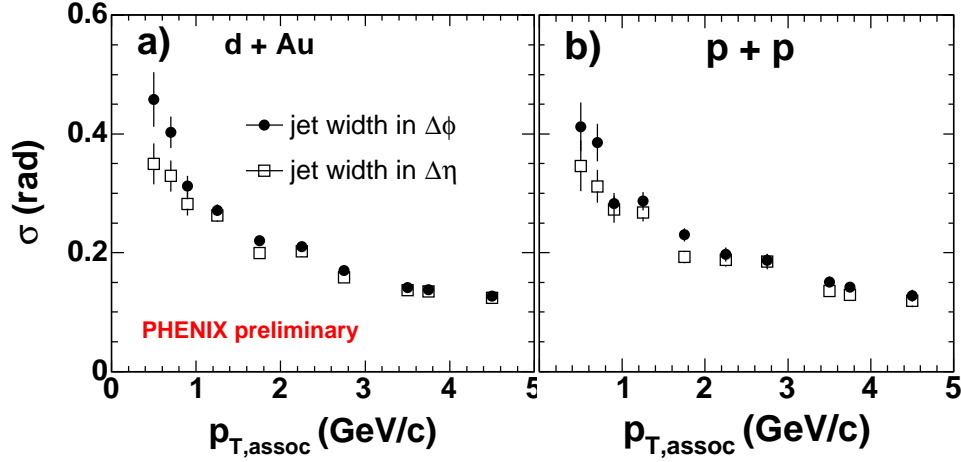


Figure 5. The comparison of jet width as function of $p_{T,assoc}$ in $\Delta\phi$ (solid circles) and $\Delta\eta$ (open boxes) from $\pi^\pm - h^\pm$ correlation. a) results for $d + Au$. b) results for $p + p$.

contribution might have been washed out by the much larger contributions from initial and final radiation, which explains the lack of difference between the two systems.

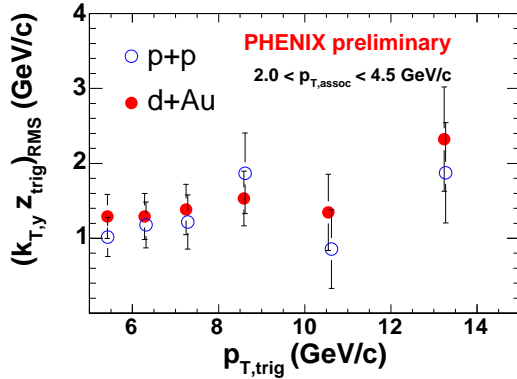


Figure 6. The comparison of $(z_{trig} k_{T,y})_{RMS}$ values between $d + Au$ (filled circles) and $p + p$ (open circles) as function of $p_{T,trig}$.

An alternative but more direct way in studying the away side k_T broadening is through the p_{out} distribution. For small angles, p_{out} has simple relation to j_T and k_T [2]:

$$\langle p_{out,same}^2 \rangle \approx \langle j_{T,y}^2 \rangle + x_E^2 \langle j_{T,y}^2 \rangle$$

$$\langle p_{out,away}^2 \rangle \approx \langle j_{T,y}^2 \rangle + x_E^2 \langle j_{T,y}^2 \rangle + 2x_E^2 \langle z^2 k_{T,y}^2 \rangle$$

Thus the difference of same side and away side p_{out} distributions directly reflects the contribution from k_T .

$$2x_E^2 \langle z^2 k_{T,y}^2 \rangle \approx \langle p_{out,same}^2 \rangle - \langle p_{out,away}^2 \rangle \quad (10)$$

Figure. 7a shows the same side and away side p_{out} distribution. There is a significant difference between the two, which reflects the contribution from k_T . Both distributions have a gauss shape at small p_{out} followed by an excess at large p_{out} . The gauss part presumably is due to the jet fragmentation (in both the same and away side) and intrinsic k_T (away side only), while the excess is evidence for hard radiation contribution of the outgoing partons. Since the away side

p_{out} carries information about k_T , we compare between $p + p$ and $d + Au$ to see whether there is hint of additional k_T broadening in $d + Au$. The comparisons of away side p_{out} distributions are shown in Figure.7b, no apparent differences are observed, consistent with the observations that $(zk_{T_y})_{RMS}$ are similar between $p + p$ and $d + Au$.

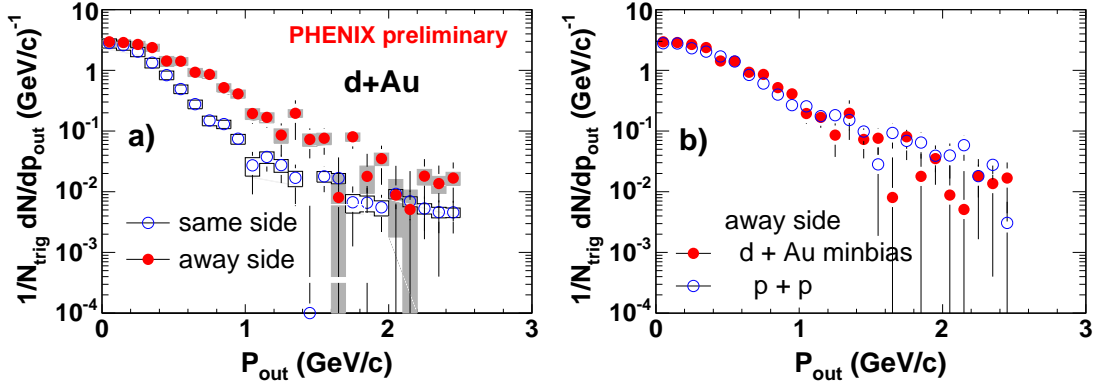


Figure 7. a) Same side and away side p_{out} distributions in $d + Au$ collisions. b) The away side p_{out} distributions compared between $p + p$ and $d + Au$.

3.2. Jet yields

The same side and away side p_T distributions of the charged hadrons associated with jets are plotted in Fig8, comparing between $p + p$ and $d + Au$ collisions. The same side yield is related to the di-hadron fragmentation, since both particles comes from the same jet, while the away side yield depends on two independent fragmentation functions: one parton fragments to produce the trigger, while the second parton produces the associated hadron. No apparent differences are seen between $p + p$ and $d + Au$; this observation is in contradiction to some recombination model prediction [11], in which a significant difference is expected due to shower-thermal contribution.

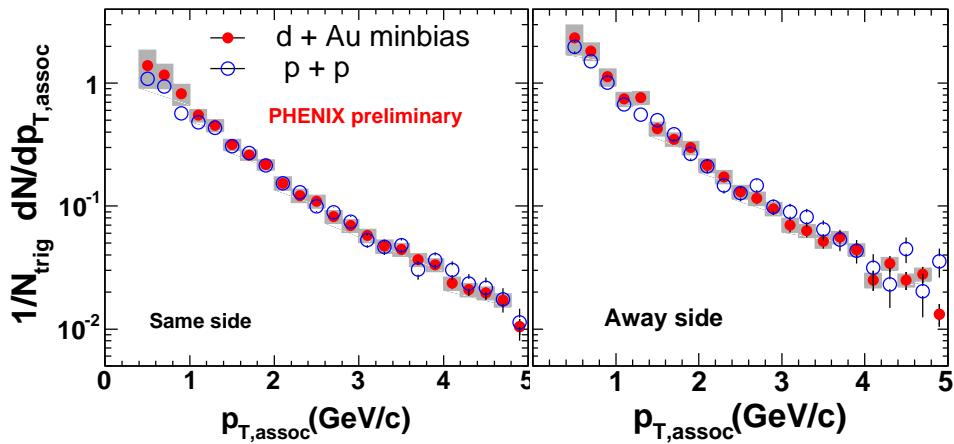


Figure 8. Jet pair distribution as function of $p_{T,assoc}$ for same side (right panel) and away side (left panel) in $p + p$ and $d + Au$.

Di-hadron correlation also gives the x_E distribution $\frac{1}{N_{trig}} \frac{dN_h}{dx_E}$, where $x_E = z_{assoc}/z_{trig}$. When di-jet p_T imbalance is ignored and $z_{assoc} \ll z_{trig}$, z_{trig} varies very slowly with z_{assoc} . Hence the x_E distribution is closely related to the fragmentation function $D(z)$,

$$\frac{1}{N_{trig}} \frac{dN_h}{dx_E} \approx z_{trig} D(z) \quad . \quad (11)$$

Figure.9 shows the measured x_E distribution between $p + p$ and $d + Au$. Again, no difference is seen between the two collision systems in both the same side and away side.

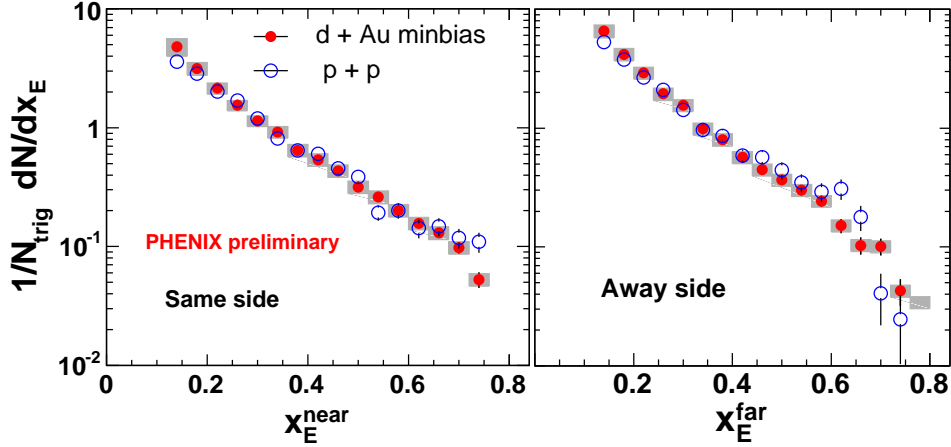


Figure 9. x_E distributions as function of $p_{T,assoc}$ for same side (right panel) and away side (left panel) in $p + p$ and $d + Au$.

In e^+e^- or $p + p$ collisions, the fragmentation functions $D(z)$ are known to approximately scale, *i.e.* are independent of jet energy. To check whether this is still true in $d + Au$ collisions, we plot in Figure. 10 the conditional yields as function of trigger p_T in different ranges of x_E for both $p + p$ and $d + Au$. The amount of variation is within $\pm 25\%$ for p_T from 5 – 12 GeV/ c with very little difference between the two systems. So we conclude that the evolution of the jet fragmentation as function of jet energy is very similar between $p + p$ and $d + Au$.

3.3. Comments on underlying event

Events triggered by high p_T hadrons not only contain particles originated from the two hard-scattered partons, but also those come from soft multiple interaction and the beam remnants. Underlying event in $p + p$ and $d + Au$ collisions refers to all hadrons except those from the two outgoing hard-scattered partons, which includes contributions from the beam remnants and initial and final state radiation [12]. The physics of the underlying event is poorly known due to its non-perturbative nature. It is often studied phenomenologically with various QCD Monte-carlo models that have been tuned to fit the data [13]. Underlying event has been studied extensively at the Tevatron energy [12, 14]. Similar studies at the RHIC are very useful in understanding its dependence on \sqrt{s} , and can provide valuable constraints on the underlying event physics at the LHC.

Figure.11 shows the jet pair distribution in $p + p$ collisions, reproduced from Figure.3. The pedestal in the $\Delta\phi$ correlation, which represents the underlying event contribution, decreases quickly and becomes negligible at $p_{T,assoc} > 2$ GeV/ c . However, the level corresponding to minimum bias $p + p$ events, denoted by the thick horizontal line, seems to decrease even faster.

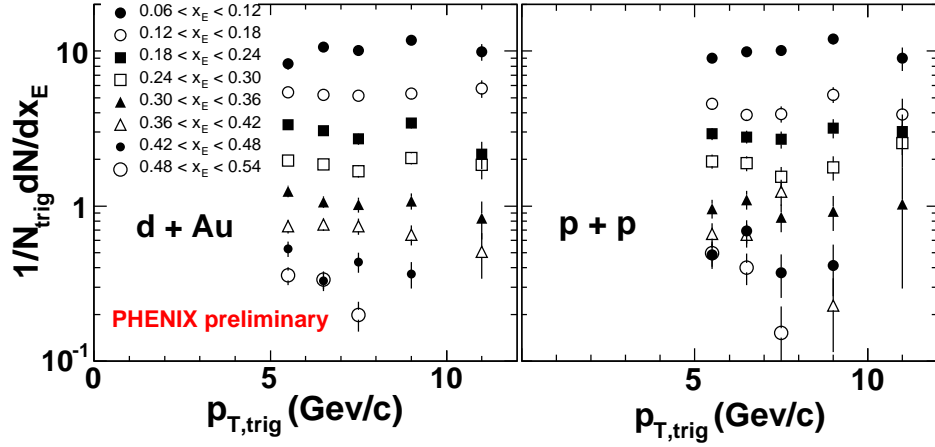


Figure 10. Away side conditional yield as function of $p_{T,\text{trig}}$ for different ranges of x_E in a) minimum-bias $d + \text{Au}$ collisions and b) $p + p$ collisions.

Since minimum bias event has small hard-scattering contribution, the relative abundance of the pedestal in triggered events over the minimum bias events indicates that most of the underlying event comes from the initial or final state radiation of the hard-scattered partons.

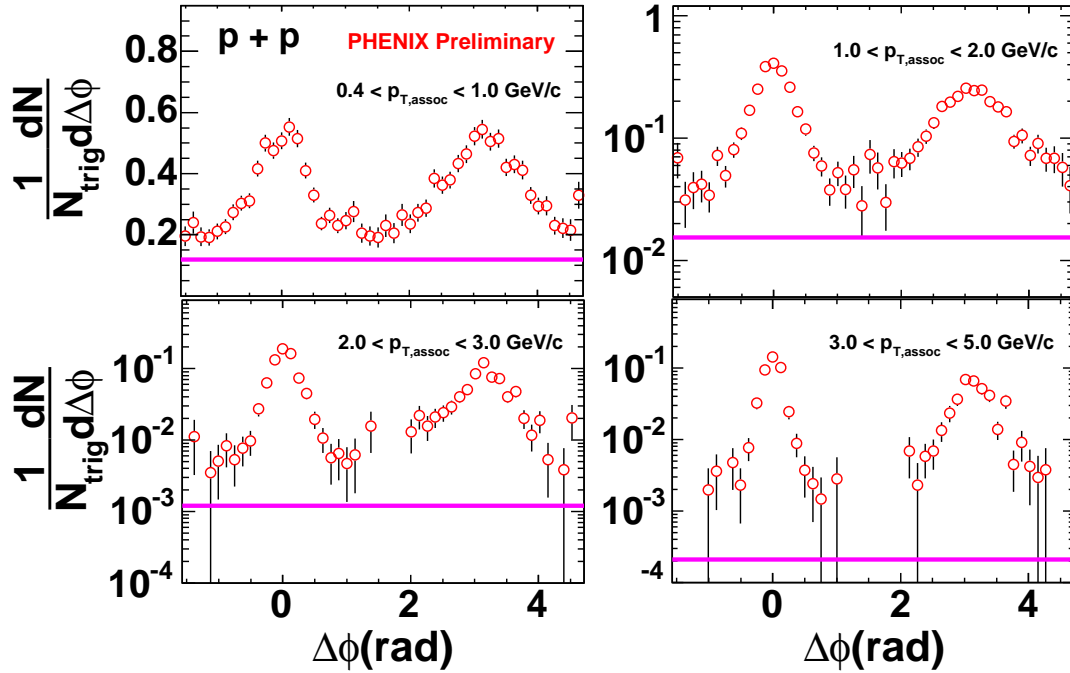


Figure 11. Corrected condition yield in $\Delta\phi$ for $p + p$ collisions (from Figure.3). The thick solid line represents the average level for minimum bias events, i.e. it is equal to $\text{Yield}_{pp}/(2\pi)$.

The underlying event at RHIC can be checked in QCD Monte-carlo models. We use the PYTHIA6.131, which seems to be able to reproduce the jet conditional yield as shown in Figure.12. The roles of the initial/final state radiations are studied by switching them on and

off in PYTHIA simulation. Figure.13a shows a typical $\pi^\pm - h^\pm$ azimuthal correlation with (top histogram) and without (bottom histogram) radiation from the simulation. There is a significant enhancement in the pedestal level when radiations are enabled. We can perform a more quantitative comparison by plotting separately the jet contribution (double gauss component), the underlying event (the constant component) and the minimum bias event level as function of p_T in Figure.13b. The hierarchy of the three contributions can be clearly seen. For event tagged with a high p_T jet, the spectra for both the jet fragmentation and the underlying events are much harder than that from typical minimum bias events. Current statistics from $p + p$ does not allow a quantitative comparison with the models yet, a much larger dataset collected from recent RHIC $p + p$ run in 2005 should help to address this question in the near future.

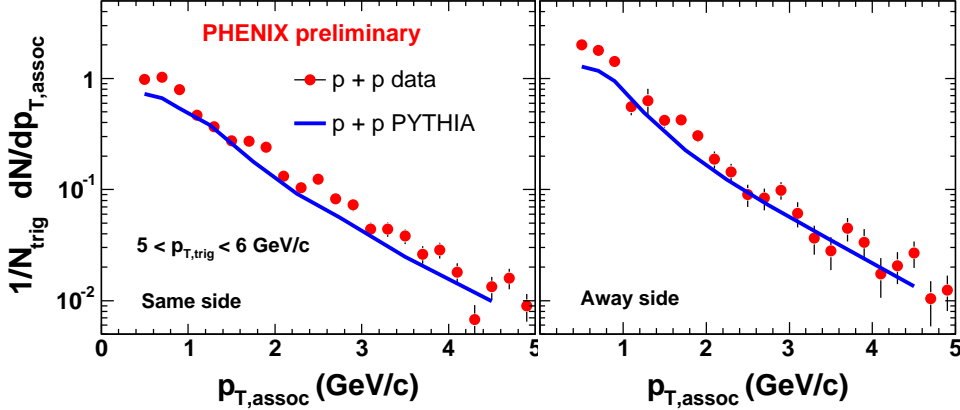


Figure 12. Conditional yield with trigger pion in $5 < p_{T,trig} < 6$ GeV/c, compared with PYTHIA 6.131 for both same side (left panel) and away side (right panel).

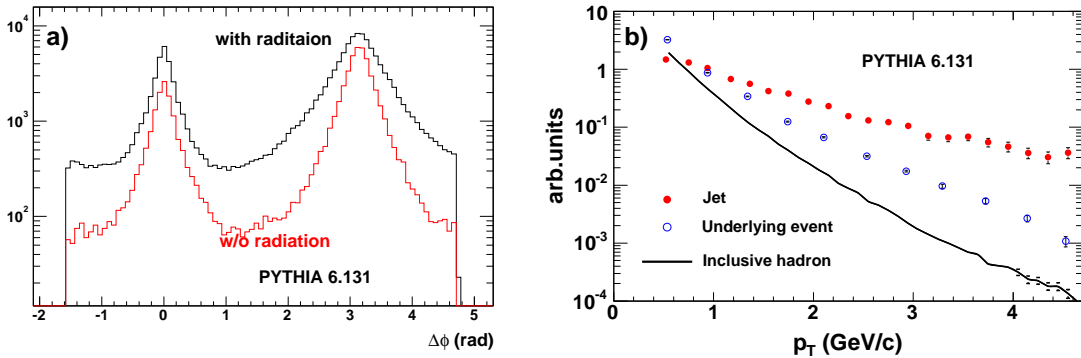


Figure 13. PYTHIA MC simulation: a) $\Delta\phi$ distribution for $3 < p_{T,assoc} < 5$ with (top histogram) and without (bottom histogram) radiation. b) the p_T spectra for jet pairs and underlying event in $p + p$ events with a > 5 GeV/c trigger, compared with minimum bias event yield.

What about the underlying event in $d + Au$? Figure.3 indicates that the underlying event levels are larger than those in $p + p$, although the properties of the jets are quite similar. Since the hard-scattering only happens in one of the nucleon-nucleon collision in $d + Au$, we can

assume the ambient particle production mechanism is the same as in minimum bias nucleon-nucleon collision. In this case, the ambient particle production should simply scale as the nuclear modification factor, R_{dAu} measured in $d + Au$ [15]. Thus the underlying event yields in $p + p$ and $d + Au$, U_{dAu} and U_{pp} are connected to each other through the following simple relation,

$$U_{dAu} = U_{pp} + R_{dAu} (N_{coll} - 1) Yield_{pp} \quad (12)$$

where $Yield_{pp}$ represents the hadron yield per event in minimum bias $p + p$ collisions. Divide both side by $Yield_{pp}$, we get,

$$\lambda_{dAu} = \lambda_{pp} + R_{dAu} (N_{coll} - 1) \quad (13)$$

$$\lambda_{dAu} = U_{dAu}/Yield_{pp}, \lambda_{pp} = U_{pp}/Yield_{pp} \quad (14)$$

note λ_{pp} denotes the ratio of underlying event yield to minimum bias event in $p + p$, which should be larger than 1 according to Figure.11 and Figure.13.

4. Conclusion

The di-jet decay kinematics are studied using $\pi^\pm - h^\pm$ correlation in $p + p$ and $d + Au$ collisions. Measured jet widths, the calculated k_T and distributions of p_{out} are very similar between $p + p$ and $d + Au$, which indicate no or small broadening in cold nuclear medium. Jet yield distribution in associated hadron p_T and x_E are also similar between $p + p$ and $d + Au$, consistent with no significant increase in jet multiplicity in $d + Au$ relative to $p + p$. The dependence of the x_E distribution on trigger p_T is weak in measured trigger p_T range. The underlying event yield in $p + p$ is studied in PYTHIA Monte-carlo. Events containing a large p_T trigger appear to have a underlying event spectra much harder than the minimum bias hadron spectra.

References

- [1] Rak J J. Phys. **G30**, S1309 (2004), hep-ex/0403038.
- [2] Jia J J. Phys. **G31**, S521 (2005), nucl-ex/0409024.
- [3] Adler C et al (STAR), Phys. Rev. Lett. **90**, 082302 (2003), nucl-ex/0210033.
- [4] Magestro D These proceedings.
- [5] Holtzmann W These proceedings.
- [6] Agakichiev G et al (CERES/NA45), Phys. Rev. Lett. **92**, 032301 (2004), nucl-ex/0303014.
- [7] Aizawa M et al (PHENIX), Nucl. Instrum. Meth. **A499**, 508 (2003).
- [8] Adler S S et al (PHENIX), Phys. Rev. **C69**, 034910 (2004), nucl-ex/0308006.
- [9] Wang X-N Phys. Rev. **C61**, 064910 (2000); Barnafoldi G G, Levai P, Papp G, Fai G I and Zhang Y Heavy Ion Phys. **18**, 79 (2003); Accardi A hep-ph/0312320; Qiu J-w and Vitev I Phys. Lett. **B570**, 161 (2003).
- [10] Boer D and Vogelsang W Phys. Rev. **D69**, 094025 (2004), hep-ph/0312320.
- [11] Hwa R C and Yang C B Phys. Rev. **C70**, 054902 (2004), nucl-th/0407081.
- [12] Affolder T et al (CDF), Phys. Rev. **D65**, 092002 (2002).
- [13] Sjostrand T and Skands P Z JHEP **03**, 053 (2004), hep-ph/0402078.
- [14] Acosta D et al (CDF), Phys. Rev. **D70**, 072002 (2004), hep-ex/0404004.
- [15] Matathias F (PHENIX) (2005), nucl-ex/0504019.